The role of promoters for Ni catalysts in low temperature (membrane) steam methane reforming

D.A.J. Michel Ligthart[a]
Johannis A.Z. Pieterse[b]
Emiel J.M. Hensen[a]

[a]Schuit Institute of Catalysis Eindhoven University of Technology, P.O. Box 513, 5600 MB Eindhoven, The Netherlands
[b]Energy Research Centre of the Netherlands (ECN), P.O. Box 1, 1755 ZG Petten, The Netherlands

Published in Elsevier 405 (2011) 108-119

ECN-W--11-066 NOVEMBER 2011

Applied Catalysis A: General 405 (2011) 108–119

Contents lists available at ScienceDirect

Applied Catalysis A: General

journal homepage: www.elsevier.com/locate/apcata

The role of promoters for Ni catalysts in low temperature (membrane) steam methane reforming

D.A.J. Michel Ligthart[a], Johannis A.Z. Pieterse[b], Emiel J.M. Hensen[a,*]

[a] Schuit Institute of Catalysis, Eindhoven University of Technology, PO Box 513, 5600 MB Eindhoven, The Netherlands
[b] Energie Centrum Nederland, P.O. Box 1, 1755 ZG Petten, The Netherlands

ARTICLE INFO

Article history:
Received 27 April 2011
Received in revised form 24 July 2011
Accepted 27 July 2011
Available online 4 August 2011

Keywords:
Steam reforming
Membranes
Nickel
Promoters
Deactivation
Coke

ABSTRACT

In the search for active and stable Ni-based catalysts for steam methane reforming in membrane reactors, the effect of three different promoters La, B and Rh was compared. Promoted and unpromoted Ni catalysts were characterized by TEM, TPR and X-ray absorption spectroscopy. The average Ni particle size is between 4 and 10 nm. Promoters affected both dispersion and reducibility of Ni. Smaller particles were found to be more difficult to reduce than larger ones. The use of B resulted in very small Ni particles. The degree of Ni reduction strongly increased by use of La and Rh promoters, whereas B strongly impeded Ni reduction. The initial intrinsic rate per surface metal atom was found to increase linearly with the Ni metal dispersion, suggesting that the rate is controlled by dissociative methane adsorption over low-coordinated surface atoms. The data indicate that Rh and La act as structural promoters to the activity. Catalysts modified by B show a much higher activity of the Ni surface atoms. Catalyst stability was investigated by using feed compositions representing the inlet of the membrane reactor and the hydrogen lean reformate towards its outlet. Stability increases in the order La < Rh < B. Deactivation of the catalysts is caused by insufficient removal of carbon species from the surface of Ni particles and the formation of stable, graphitic carbon deposits, most likely covering the surface of metal. This is substantially suppressed when the Ni particles are small. B is an excellent structural promoter to obtain small Ni particles, Rh stabilizes metallic Ni and La aids in the removal of some of the carbon deposits more effectively by gasification.

© 2011 Elsevier B.V. All rights reserved.

1. Introduction

Industrial scale production of hydrogen for power generation and fuel refineries is dominated by the catalytic reforming of natural gas and higher hydrocarbons [1,2]. With an increasing demand for hydrogen and power in the decades to come, steam reforming will likely gain further in importance. In the principle reaction light hydrocarbons, in particular methane, are converted with steam into synthesis gas (syngas). Primary reformer units are typically operated at severe conditions of high temperatures and pressure, which strongly affect the long-term performance of the classical Ni-based catalysts and the process efficiency. As an alternative, membrane reactors are being studied for pre-combustion decarbonization of methane. Membrane reactors, which selectively permeate hydrogen at operation temperatures below 600 °C to avoid membrane disintegration risks and lifetime deterioration, produce a hydrogen stream, which can be used as a fuel in a turbine combined-cycle plant, and a CO_2 rich stream for compression and storage [3,4]. High efficiency of these processes requires catalysts that are sufficiently active at temperatures in the range of 500–600 °C.

Recently, Pieterse et al. [4] reported that Ni-based catalysts provide sufficient activity for use in membrane steam reforming reactors, but their resistance to deactivation needs further improvement. Deactivation of Ni-based catalysts is related to high tendency towards coke formation and sintering of the active metal phase [5]. The former can be suppressed by increasing the steam-over-methane ratio (S/C), but by doing so sintering is often enhanced. More steam requires more heat, which makes the process less energy efficient. The S/C ratio will, therefore, practically be limited to 3. Catalysts based on noble metals like Ru [6,7], Rh [8,9], Ir [10], Pt [11,12] and Pd [13] have promising catalytic properties and a lower propensity to coke formation than Ni, but they are more expensive. Another approach is to deactivate the sites that lead to carbon formation. Pioneering work by the groups of Rostrup-Nielsen and Nørskov [14–17] for Ni-based catalysts has led to a detailed understanding about the role of potassium [18], sulfur [19] or gold [20] to suppress nucleation sites for coke formation. These additives preferentially bind to the step edge sites and thereby suppress the activity of the carbon nucleation sites [17], but concomitantly also lower the activity.

* Corresponding author. Tel.: +31 40 2475178; fax: +31 40 2455054.
E-mail address: e.j.m.hensen@tue.nl (E.J.M. Hensen).

0926-860X/$ – see front matter © 2011 Elsevier B.V. All rights reserved.
doi:10.1016/j.apcata.2011.07.035

This approach has led to follow-up work [21] with tin and boron being interesting alternative promoters. Sn seems to displace uncoordinated Ni atoms from the Ni edge to form checkerboard structure assemblies that prevent formation of carbon nucleation sites by strong hindrance of C atom diffusion and comparatively less hindrance of O atom diffusion [22]. B shows a comparable tendency to bind to Ni as C and is therefore argued to selectively block step but also subsurface sites [23]. Other additives that have been found useful in reforming reactions of methane by Ni catalysts are Rh [24–26], Pt [26–28], Pd [26,29], Ba [30] and La [31–33]. Noble metals are known for their higher carbon tolerance, whilst the latter two promoters are part of the basic metal group elements known to enhance carbon gasification [34,35].

The present study aims to obtain insight in the potential of promoted Ni-based catalysts for steam methane reforming (SMR) in membrane reactors. $MgAl_2O_4$-supported Ni catalysts modified with La, B or Rh have been prepared and are compared to their corresponding monometallic materials. The support material can stabilize small Ni particles. These catalysts exhibit a higher resistance against coking as compared to pure Al_2O_3 supported catalysts [36,37]. As promoters have been chosen (i) La forming oxycarbonate type species ($La_2O_2CO_3$) [38] and thus aiding in the minimization of coke accumulation by water activation (coke gasification [39]) or its influence on the metal dispersion [40]; (ii) B, which has been proposed to block subsurface sites and prevent carbon diffusion into the bulk [23,41] or to serve as a structural promoter [42] and (iii) Rh, which is considered to be a very active metal for SMR and able to stabilize metallic Ni [43] and inhibit coke formation [44,45]. B- and Rh-promoted Ni catalysts were also suggested to be more sulfur-tolerant than the unpromoted material [46–48]. As it will be shown that some promoters also influence the Ni particle size, we also prepared a Ni catalyst with smaller particles by homogeneous-deposition precipitation than obtained by regular impregnation. The catalysts have been characterized for their textural properties, metal particle size, reduction behavior and their activity and stability under conditions that represent the conditions at a membrane SMR reactor inlet and outlet.

2. Experimental methods

2.1. Support materials and catalysts preparation

A commercial $MgAl_2O_4$ carrier material (MkNano, 99.5%, average particle size 30 nm, surface area 52 m^2/g, pore volume 0.34 ml/g) was used for the preparation of 20 and 30 wt% Ni catalysts by pore volume impregnation. Another 20 wt% Ni catalyst was prepared by homogeneous deposition precipitation (HDP) of nickel nitrate ($Ni(NO_3)_2{\cdot}6H_2O$, Merck, >97%) on the same carrier. La_2O_3 was made by thermal decomposition of lanthanum nitrate ($La(NO_3)_3{\cdot}6H_2O$, Sigma–Aldrich, 99.999%) in static air at 625 °C with 7 °C/min for 5 h. A 20 wt% Ni catalyst was prepared on a La_2O_3 support by homogeneous precipitation of nickel nitrate. For the HDP preparation method an appropriate amount of the support material and nickel nitrate was suspended in 0.6 L deionized water and the pH was adjusted to 1.9 with HNO_3. After addition of 80 ml of 1 M urea (Merck, 99%), the mixture was heated under stirring in a double-walled vessel at 95 °C for 18 h. Subsequently, the precipitate was filtered and washed with deionized water, dried in an oven and calcined.

La- and B-promoted Ni catalysts were prepared by sequential impregnation. The La–$MgAl_2O_4$ support was prepared by pore volume impregnation with an aqueous solution of lanthanum nitrate. After impregnation, the material was dried in air, in an oven overnight and subsequently impregnated with the nickel nitrate solution to obtain a Ni/La molar ratio of 4.7, which was determined to be the optimal one [49]. Two Ni catalysts were promoted by B following a procedure described by Saeys and coworkers [23]. The support was first impregnated with a nickel nitrate solution, followed by a drying period of 3 h in air and overnight at 110 °C. After calcination in 20 vol.% O_2 in N_2 to 625 °C at a rate of 2 °C/min for 5 h, boric acid (H_3BO_3, Merck, 99.9999% Suprapur) was introduced at a Ni/B ratio of 2.7. Two Rh-promoted Ni catalysts were prepared by co-impregnation with a solution of Rh and Ni nitrates to obtain Ni/Rh molar ratios around 70 and 22. The impregnated materials were dried in air and in an oven at 110 °C before calcination.

Reference catalysts containing 0.5 wt% Rh, 10 wt% La or 2 wt% B supported on $MgAl_2O_4$ were prepared for comparison. $LaNiO_3$ was synthesized according to the sol gel method [50]. Stoichiometric amounts of $La(NO_3)_3{\cdot}6H_2O$ and $Ni(NO_3)_2{\cdot}6H_2O$ were dissolved in distilled water and added to a solution containing equimolecular amounts of citric acid (Sigma–Aldrich, >99.5%) and ethylene glycol (Sigma–Aldrich, >99%) as a polydentate ligand. Excess water was slowly removed in a rotary-evaporator until a viscous liquid was obtained. This solution was then dried overnight in an oven at 90 °C and slowly crystallized in air by heating to 800 °C with a rate of 1 °C/min and an isothermal period of 5 h. $La_2O_2CO_3$ was synthesized from La_2O_3 via carbonation with 10 ml/min CO_2 flow to 600 °C with 6 °C/min for 3 h. This material was then cooled to room temperature in CO_2 flow [51,52].

All catalysts were sieved into a fraction of 125–250 μm and calcined in a mixture of 20 vol.% O_2 in N_2 (except for $La_2O_2CO_3$) at a flow rate of 100 ml/min, whilst heating at a rate of 2 °C/min to 625 °C followed by an isothermal period of 5 h. The surface area is typically around 34 and 4 m^2/g for the $MgAl_2O_4$- and La_2O_3-supported materials, respectively.

The catalysts are denoted by Ni(x)P(y)/S-HDP, where P, S, x and y represent the promoter (La, B or Rh), support ($MgAl_2O_4$ or La_2O_3), the weight percentage of Ni and the promoter, respectively. The optional postfix HDP refers to the use of the homogeneous deposition precipitation method.

It has been confirmed that the textural and structural properties of the support materials did not change following calcination and reduction steps of the final catalysts.

2.2. Characterization

2.2.1. ICP analysis

The metal loading was determined by inductively coupled plasma atomic emission spectroscopy (ICP-AES) analyses performed on a Goffin Meyvis SpectroCirus apparatus. Typically, an amount of sample was dissolved in a 1:1 H_2O/H_2SO_4 solution under heating until a clear solution was obtained. For a selected number of catalysts it was confirmed that calcination followed by reduction and passivation did not result in a change of the metal loading.

2.2.2. Nitrogen physisorption

Surface areas were measured with a Micromeritics TriStar 3000 apparatus by nitrogen physisorption at −196 °C after outgassing the sample for 3 h under vacuum at 150 °C

2.2.3. Hydrogen chemisorption

Chemisorption of the Rh catalyst was carried out at −80 °C using a Micromeritics ASAP 2020C setup equipped with an isopropanol bath cooled by a thermostat. The sample was first reduced at 600 °C (heating rate 1.2 °C/min) for 5 h and evacuated for 4.5 h. The double isotherm method with an intermediate vacuum treatment of 1 h was employed. An adsorption stoichiometry of one H per surface Rh atom was assumed.

2.2.4. Transmission electron microscopy (TEM)

Transmission electron micrographs were acquired on a FEI Tecnai 20 transmission electron microscope at an acceleration voltage

of 200 kV with a LaB6 filament. Typically, a small amount of grinded sample was reduced at 600 °C and passivated in 1 vol.% O_2 in He for 2 h before being suspended in pure ethanol, sonicated and dispersed over a Cu grid with a holey carbon film. TEM images were recorded using a CCD camera at different magnifications. From the electron micrographs, the particle size was determined assuming that the particles are spherical. The particle size distributions followed by analysis of at least 150 particles from at least three different micrographs

2.2.5. Temperature-programmed reduction (TPR)

TPR experiments were carried out in a flow apparatus equipped with a fixed-bed reactor, a computer-controlled oven and a thermal conductivity detector. Typically, an amount of catalyst was contained between two quartz wool plugs in a quartz reactor. Prior to TPR, the catalyst was oxidized by exposure to a flowing mixture of 4 vol.% O_2 in He whilst heating to 110 °C at a rate of 10 °C/min. After the sample was cooled to room temperature in flowing N_2, the sample was reduced in 4 vol.% H_2 in N_2 at a flow rate of 8 ml/min, whilst heating from room temperature up to 800 °C at a rate of 10 °C/min. The H_2 signal was calibrated using a CuO/SiO_2 reference catalyst.

2.2.6. X-Ray absorption spectroscopy

X-Ray absorption measurements were carried out at the Dutch–Belgian Beamline (Dubble) at the European synchrotron radiation facility (ESRF), Grenoble, France (storage ring 6.0 GeV, ring current 200 mA). Data were collected at the Ni K-edge in transmission mode. The Rh K-edge was measured in fluorescence mode with a 9-channel solid-state detector. Energy selection was done by a double crystal Si (1 1 1) monochromator. The near-edge region of the absorption spectra of the reference compounds (Ni foil, NiO, $LaNiO_3$, Rh foil and Rh_2O_3) was used to fit the experimental near-edge spectra.

Spectra at the Ni and Rh K-edges were recorded in a stainless-steel controlled atmosphere cell. Typically, an amount of 25 mg for the Ni-containing catalysts (200 mg for Rh) was pressed in a stainless-steel holder and placed in the cell to give an absorption μx of about 2.5. High-purity carbon windows with a thickness of 200 and 1000 μm were held between high-purity carbon spacers for experiments at 1 and 5 bar, respectively. Gases were supplied by thermal mass flow controllers with steam being generated by a controlled evaporator mixer unit. The total gas flow was kept at 50 ml/min. All transfer lines were kept at 125 °C after the point of steam introduction to avoid condensation. At the outlet, steam was condensed and the composition of the dry gas was analyzed by a Micro-GC (Agilent) system equipped with a Porapak Q column with a thermal conductivity detector. The effluent mixture was found to be at thermodynamic equilibrium under these conditions. Catalysts were ex situ reduced at 600 °C (heating rate 1.2 °C/min) for 5 h and passivated in 1 vol.% O_2 in He for 3 h at ambient temperature. The catalysts were re-reduced in situ by heating to 600 °C at a rate of 10 °C/min whilst recording XANES spectra. Finally, XANES spectra were recorded during conventional reforming and simulated membrane reforming.

2.2.7. Analysis carbonaceous deposits

Temperature-programmed oxidation (TPO) was employed to quantify the amount of carbonaceous deposits in a microflow system attached to a Balzers mass spectrometer. These deposits were produced by exposure of the reduced catalyst to various gas mixtures, namely (i) CH_4 in He, (ii) CH_4/H_2 in He, (iii) CO in He or (iv) CO_2 in He. In a typical experiment, 100 mg of sample was loaded into a quartz reactor tube and kept between two layers of quartz wool. The sample was reduced in a mixture of 20 vol.% H_2 in He, whilst heating from room temperature to 600 °C at a rate of 1.2 °C/min followed by an isothermal period of 5 h (10 °C/min for 2 h for $MgAl_2O_4$). After reduction, the catalyst was purged with He for 15 min and subsequently exposed to a flow of 100 ml/min of the desired gas mixture for carbon laydown for a certain period. The sample was then purged with He and rapidly cooled to room temperature. The removal of gases was monitored by online mass spectrometry. TPO was carried out by heating the sample to 800 °C at a rate of 10 °C/min with 6 vol.% O_2 in He. The CO_2 signal was calibrated by following the decomposition of a well-known amount of $NaHCO_3$ (Acros, >99.5%).

Table 1
Gas composition (vol.%) of the reaction feed mixtures for steam methane reforming.

Mode	CH_4	H_2O	H_2	CO	CO_2
RF	5	15	0	0	0
MR	1.35	15	3	0.14	11.75

2.3. Catalytic activity in steam methane reforming

The catalytic activity in SMR was measured using a fixed-bed microflow reactor system. The stainless steel reactor tube with an internal diameter of 6 mm was placed in a brass body to ensure isothermal operation of the reactor. The catalyst (sieved to 125–250 μm) was mixed with inert α-Al_2O_3 (99.997%, 110 μm crystalline, surface area 5.5 m^2/g) to obtain a bed height of about 20 mm. A stainless steel rod was used to fix the position of the bed between two plugs of quartz wool in the isothermal region of the oven. Prior to catalytic activity measurements, the catalysts were reduced in 20 vol.% H_2 in N_2 by heating to 600 °C at a rate of 1.2 °C/min followed by an isothermal period for 5 h. After reduction, the catalyst was purged with N_2 before exposure to the reaction mixture. SMR was carried out at 600 °C and 1.2 bar. Two different reactor feed compositions were employed (Table 1): (i) for conventional reforming with H/C = 10 and O/C = 3 and (ii) for membrane reforming with H/C = 3 and O/C = 3. Hereafter, conventional and membrane reforming will be denoted as RF and MR, respectively. The composition of the effluent gas was analyzed by online gas chromatography (Interscience GC-8000 Top) equipped with a ShinCarbon ST 80/100 packed column (2 mm × 2 m) and a thermal conductivity detector.

The gas composition of MR is obtained on the basis of thermodynamic calculations of equilibrium gas compositions at 600 °C after RF to simulate the removal of hydrogen by a membrane. The composition corresponds to a methane conversion of 91% of a feed containing 7.5 vol.% CH_4 and 22.5 vol.% H_2O with a large part of the H_2 product removed [4]. The hydrogen concentration was set to 3 vol.%. These choices for the feed compositions allow to compare reactions in conventional reforming (high H/C ratio) and simulated membrane reforming (low H/C ratio) at constant O/C ratio and represent the situation at the inlet and outlet of a membrane reactor [4]. A space velocity in the range of 0.8–3 × 10^6 $cm^3/(h\,g_{cat})$ was used. Steam was supplied by evaporation of deionized water in a Controlled Evaporator Mixer unit in combination with a liquid-flow controller (Bronkhorst) and gas flows were controlled by mass flow controllers (Brooks). All tubings were kept at 125 °C after the point of steam introduction to avoid condensation. The conversion was calculated from the effluent concentrations via [34]:

$$X_{CH_4} = \frac{[CO]_{out} + [CO_2]_{out}}{[CH_4]_{out} + [CO]_{out} + [CO_2]_{out}} \quad (1)$$

and/or

$$X_{CH_4} = 1 - \frac{[CH_4]_{out}}{[CH_4]_{in}} \quad (2)$$

The latter expression is used for MR experiments, because of the very small amounts of co-fed gases. For RF experiments, application of Eqs. (1) and (2) gave similar results.

The forward CH_4 turnover rates (r_f) were calculated by correction of the measured net reaction rate (r_n) for approach to the thermodynamic equilibrium (η) [53] using

$$r_f = \frac{r_n}{(1-\eta)} \quad (3)$$

with

$$\eta = \frac{[P_{CO}][P_{H_2}]^3}{[P_{CH_4}][P_{H_2O}]}\frac{1}{K_{eq}},$$

P_i the pressure of species i (bar) and K_{eq} the equilibrium constant of the reforming reaction. These corrections were minor with typical initial values of η around 0.2 for the catalyst with the highest Ni loading. The rate of CH_4 consumption in the reactor was determined based on the CH_4 inlet flow. Finally, the rate for reforming is described by

$$r_f = k(T)P_{CH_4} \quad (4)$$

3. Results and discussion

3.1. Catalyst characterization

Table 2 lists the most important properties of the catalysts. For comparison, a number of non-promoted catalysts have been included. For the study of lanthanum promotion, Ni(20)/La_2O_3-HDP and $LaNiO_3$ were used as reference catalysts. The final Ni/La molar ratio of the La-promoted Ni catalyst (Ni(20)La(10)/$MgAl_2O_4$) is 4.8. The Ni/B molar ratio of the two B-promoted Ni catalysts is around 2.8. The two Rh-promoted Ni catalysts have a final Ni/Rh molar ratio of 58 and 18.

The particle size of the active Ni phase was determined by TEM. Fig. 1 shows representative transmission electron micrographs and particle size distributions of the monometallic Ni catalysts. The Ni particles become larger and the particle size distribution broadens with increasing Ni loading. As expected, the HDP method results in smaller Ni crystallites as compared to conventional impregnation. The HDP catalyst (Ni(20)/$MgAl_2O_4$-HDP) contains particles in the range 3–6 nm. It is not possible to accurately determine the Ni crystallite size of Ni(20)/La_2O_3-HDP due to the lack of contrast between Ni and La. From inspection of particles visible at the edges of the support, the Ni particles appear to be in the 4–6 nm range. The TEM images of Rh(0.5)/$MgAl_2O_4$ show very finely dispersed Rh particles with an average particle size of 1.4 nm in agreement with the value determined by H_2 chemisorption (Table 2).

Fig. 2 shows representative transmission electron micrographs and corresponding particle size distributions of the promoted Ni catalysts. The average Ni particle size of Ni(20)La(10)/$MgAl_2O_4$ is lower than that of its unpromoted counterpart. This difference agrees with the findings of Zhang et al. [54], who found smaller particles in La-promoted Ni/Al_2O_3 than in Ni/Al_2O_3. Promotion with B has a much more pronounced effect on the particle size. The average particle size is 4.6 and 6.4 nm for the 20 and 30 wt% Ni catalysts, respectively, as compared to the initial sizes of 8.1 and 10.3 nm before B promotion. Broadly speaking, this agrees with the findings of Dautzenberg and co-workers [42], who found a decrease from 15–25 nm to 8–10 nm upon B promotion. In contrast, Xu et al. [23] reported that the Ni particle size did not vary upon B promotion. The use of a small amount of Rh also led to a small decrease of the Ni particle size, which became more pronounced when more Rh was added. However, these changes are relatively small as compared to the effect of B.

Fig. 3 shows TPR traces of the supports and the catalysts. Expectedly, no reduction features are seen for $MgAl_2O_4$. The reduction of the $MgAl_2O_4$-supported Ni catalysts started around 375 °C and reached completion around 800 °C. It is seen that the NiO reduction takes place at lower temperature for higher Ni content, which is due to the weaker support interaction of larger NiO crystallites. To have a basis of comparison, the Ni-free promoter-containing supports are also included. The reducibility of La-containing supports is negligible and only a weak high temperature feature is observed for B(2)/$MgAl_2O_4$. The reduction of Rh(0.5)/$MgAl_2O_4$ occurs below 400 °C, which is substantially higher than that of Rh particles dispersed over ceria or zirconia [55]. This is due to the comparatively strong interaction with alumina [56]. The TPR trace of Ni(20)/La_2O_3-HDP contains a dominant feature around 400 °C, which is also present in the reduction of $LaNiO_3$. The reduction of the latter compound is known to proceed in two consecutive steps [57], *i.e.* (i) reduction of Ni^{3+} to Ni^{2+} with concomitant formation of $La_2Ni_2O_5$ and (ii) reduction of Ni^{2+} to metallic Ni and La_2O_3. Accordingly, it is reasonable to suggest that during calcination

Table 2
Catalyst labeling, metal loading, metal dispersion.

Catalyst label	Ni loading[a] (wt%)	Promoter loading[a] (wt%)	d[b] (nm)	D[c] (%)
Ni(20)La(10)/$MgAl_2O_4$	16.3	8.11	7.2 ± 1.8	14
Ni(20)B(1.4)/$MgAl_2O_4$	17.8	1.16	4.6 ± 1.2	22
Ni(30)B(2)/$MgAl_2O_4$	29.2	1.79	6.4 ± 1.9	15.8
Ni(20)Rh(0.5)/$MgAl_2O_4$	18.1	0.55	7.5 ± 2.6	13.5
Ni(20)Rh(1.6)/$MgAl_2O_4$	18.2	1.73	6.2 ± 2.0	16.3
Ni(20)/$MgAl_2O_4$	17.8	–	8.1 ± 3	12.5
Ni(30)/$MgAl_2O_4$	29.2	–	10.3 ± 3.4	9.8
Ni(20)/$MgAl_2O_4$-HDP	19.2	–	4.5 ± 1.6	22.5
La(10)/$MgAl_2O_4$	–	9.65	–	–
B(2)/$MgAl_2O_4$	–	2.04	–	–
Rh(0.5)/$MgAl_2O_4$	–	0.61	1.4 ± 0.4 (1.2)[d]	78
$MgAl_2O_4$	–	–	–	–
La_2O_3	–	–	–	–
Ni(20)/La_2O_3-HDP	20.4	–	*n.d.*[e]	*n.d.*[e]
$LaNiO_3$	–	–	–	–

[a] Determined by ICP-AES with La, B, Rh promoters.
[b] Average particle size, standard deviation determined by TEM analysis (Ni + promoter, Ni).
[c] Dispersion.
[d] Determined by H_2-chemisorption.
[e] Not determined: limited detection of particles.

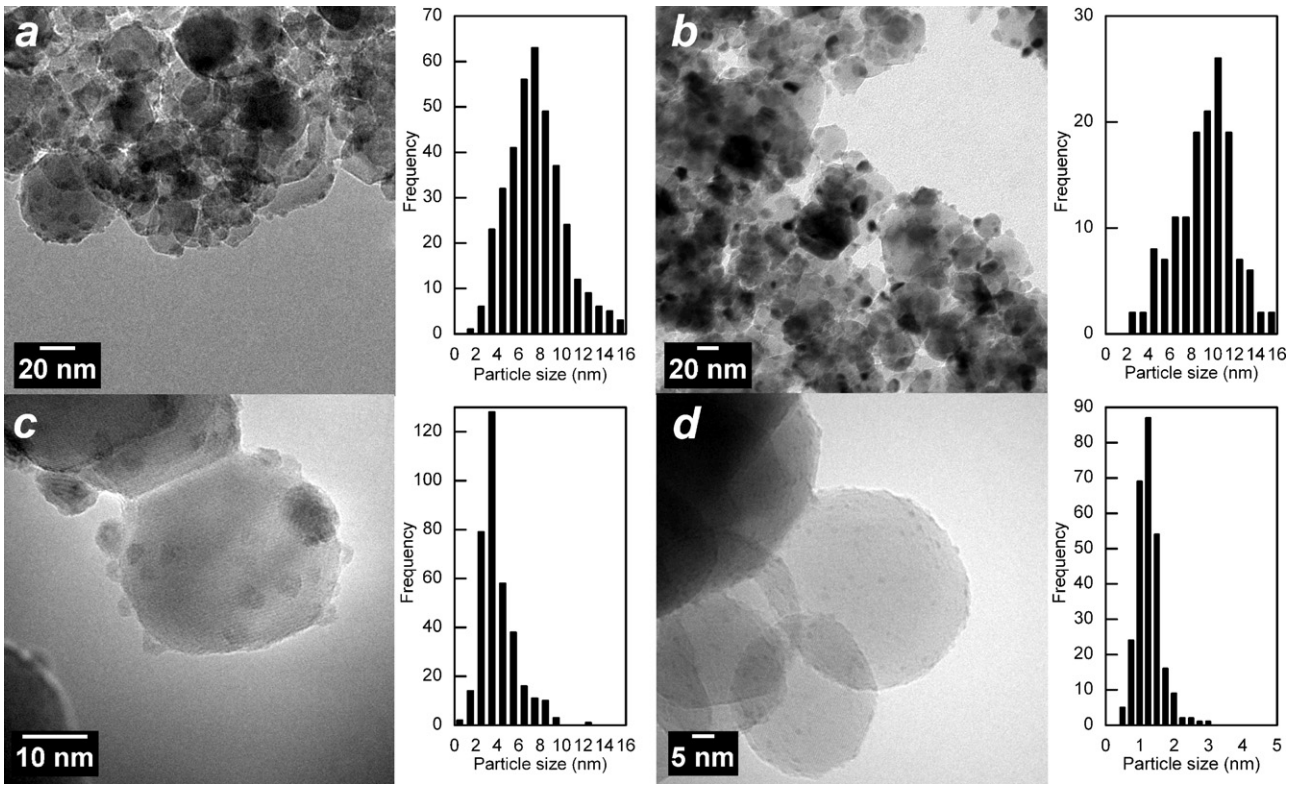

Fig. 1. Transmission electron micrographs, Ni particle size distributions of (a) Ni(20)/$MgAl_2O_4$, (b) Ni(30)/$MgAl_2O_4$, (c) Ni(20)/$MgAl_2O_4$-HDP, (d) Rh(0.5)/$MgAl_2O_4$ with average particle diameters of 8.1, 10.3, 4.5, 1.4 nm, respectively.

of Ni(20)/La_2O_3-HDP $LaNiO_3$ is formed. This reduction feature is absent in the TPR trace of Ni(20)La(10)/$MgAl_2O_4$.

Interestingly, the TPR traces of the two B-promoted catalysts only show a reduction feature at very high temperature. As can be deduced from the intensities of the bands, the reduction must be due to nickel oxide reduction. The high temperature points to a very strong Ni–B interaction. It has been shown before that Ni and B become alloyed upon calcination [58,59]. More recently, DFT calculations have indicated that boron binds preferentially to step sites and octahedral sites just below the surface of Ni metal [60]. The low-temperature shoulder in the trace of Ni(30)B(2)/$MgAl_2O_4$ may correspond to the reduction of some NiO particles that have not been alloyed with B. Finally, the Ni–Rh catalyst with the lower Rh content shows a quite similar trace to that of its Ni-free counterpart. The small reduction feature below 400 °C for the catalyst with a higher Rh content relates to Rh reduction [26]. These data suggest that at these metal loadings an alloy is formed. Earlier, Song and co-workers reported that Ni and Rh reduction proceed in two consecutive steps, but the Rh loading in that case was much higher [48].

The results of a quantitative analysis of the TPR data are given in Table 3. It is seen that the extent of reduction of $MgAl_2O_4$-supported catalysts depends on the promoter and increases in the order B < no promoter < La < Rh. Importantly, Table 3 also contains the fraction of reduced Ni (f_{Ni}) after reduction at 600 °C during the TPR experiment. Obviously, the TPR experiments signify that Ni reduction of the B-promoted catalysts is very difficult and one may argue that after reduction at 600 °C for prolonged time the fraction of reduced Ni will be smaller than that of the other materials. The Rh-containing catalysts are nearly completely reduced, whilst the reduction of larger particles is more extensive than that of smaller ones.

The reduction behavior of a few catalysts has also been measured by in situ XANES. Ni near-edge spectra at various reduction temperatures of pre-reduced and passivated Ni(20)/$MgAl_2O_4$-HDP, Ni(20)/$MgAl_2O_4$ and Ni(20)La(10)/$MgAl_2O_4$ are collected in Fig. 4. The best fit spectra are included as determined by a least-squares fit with Ni metal and NiO reference XANES data. At room temperature these catalysts contain a whiteline at ~2 eV above the edge, which is typical for Ni^{2+}. This feature decreases in intensity with increasing temperature, indicating that a larger proportion of the Ni atoms becomes metallic. The whiteline is nearly absent for Ni(20)La(10)/$MgAl_2O_4$. Fig. 5 shows the fraction of oxidic Ni and Rh ($f_{Ni_{2+}(Rh^{3+})}$) with temperature. These catalysts were pre-reduced at 600 °C, then passivated and exposed to air before the XANES experiment with the exception of Rh(0.5)/$MgAl_2O_4$, which was reduced in situ. To start with the latter, the reduction occurs over a broad temperature range up to 600 °C. Rh reduction is nearly complete at the final temperature and exposure to gas RF and MR conditions does not bring about changes to its oxidation state.

The reduction degree of passivated Ni(20)/$MgAl_2O_4$-HDP is nearly 60% and further reduction leads to a final reduction

Table 3
TPR results (temperature, H_2 consumed, H_2/Ni ratios) of the set of catalysts.

Catalyst	H_2 uptake (mmol/g_{cat})	H_2/Ni[a]	f_{Ni}[b]
Ni(20)La(10)/$MgAl_2O_4$	2.8	1	0.74
Ni(20)B(1.4)/$MgAl_2O_4$	2.35	0.77	0.09
Ni(30)B(2)/$MgAl_2O_4$	3.81	0.77	0.12
Ni(20)Rh(0.5)/$MgAl_2O_4$	1.9	1.08	0.83
Ni(20)Rh(1.6)/$MgAl_2O_4$	2.31	1.3	1
Ni(20)/$MgAl_2O_4$	2.54	0.84	0.48
Ni(30)/$MgAl_2O_4$	4.82	0.97	0.7
Ni(20)/$MgAl_2O_4$-HDP	2.75	0.84	0.43
Ni(20)/La_2O_3-HDP	4.03	1.16	–

[a] Based on Ni loading; reduced up to 800 °C.
[b] Fraction of metallic Ni after reduction up to 600 °C.

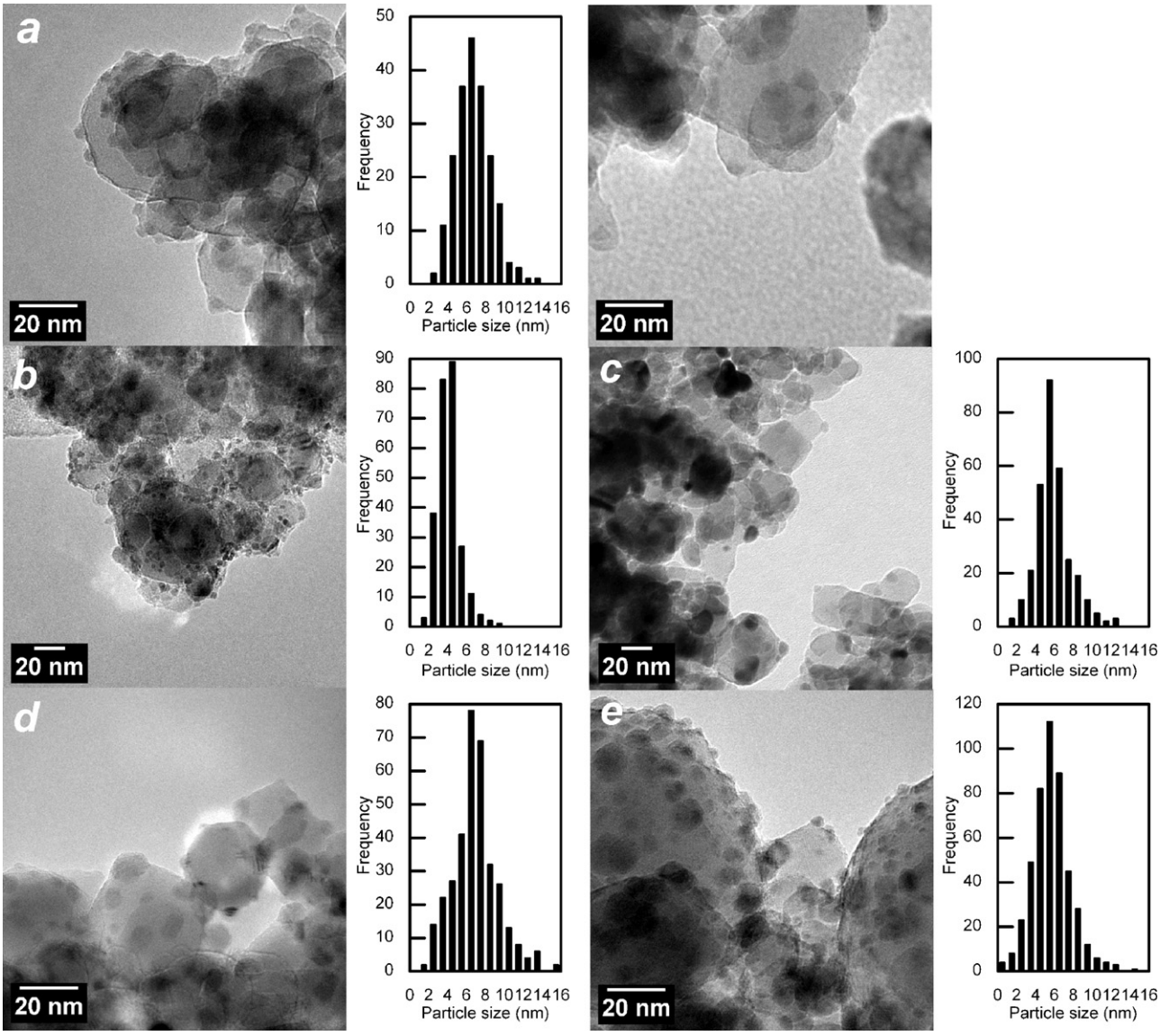

Fig. 2. Transmission electron micrographs, particle size distributions of (a) Ni(20)La(10)/$MgAl_2O_4$, (b) Ni(20)B(1.4)/$MgAl_2O_4$, (c) Ni(30)B(2)/$MgAl_2O_4$, (d) Ni(20)Rh(0.5)/$MgAl_2O_4$, (e) Ni(20)Rh(1.6)/$MgAl_2O_4$ with average particle diameters of 7.2, 4.6, 6.4, 7.5, 6.2 nm, respectively.

degree of about 75%. These values are somewhat higher than the kinetic result obtained by TPR. Compared to this, the reduction of Ni(20)/$MgAl_2O_4$ amounts to 55% after re-reduction from an initial reduction degree of nearly 30%. The higher reduction degree of Ni(20)/$MgAl_2O_4$ in comparison to the HDP sample is in reasonable agreement with the TPR results. The La-promoted catalyst is nearly completely reduced. In those cases that reduction of the Ni phase is not complete, it is seen that steam reforming under RF or MR conditions leads to a gradual increase of the reduction degree. This is in line with the TPR results that indicate that the Ni phase is still reducing at 600 °C. It should be noted that the catalysts were reduced at 600 °C for 5 h prior to catalytic activity testing for steam methane reforming and, accordingly, one may argue that the final Ni reduction degrees are close to the values after MR testing.

3.2. Catalyst activity measurements

The catalysts were tested for their activity and stability in SMR under the following conditions: 15 h RF (RF1), 20 h MR (MR1), 2.5 h RF (RF2) and 2.5 h MR (MR2). The reaction rate is corrected for the metal dispersion and the fraction of the active phase in its metallic form in order to make meaningful comparisons. For the Ni dispersion we used values determined by TEM analysis. This introduces only a small error because the promoter content is small in all cases. Similar to the method outlined by Wei and Iglesia [53], the fraction of metallic Ni as determined by TPR after reduction at 600 °C was used to correct for the amount of non-reduced Ni. Accordingly, an intrinsic activity per surface atom can be calculated.

Fig. 6 shows the initial intrinsic activities as a function of the Ni dispersion. The initial reaction rate increases linearly with the dispersion. In accordance with our earlier results, this finding implies that the overall SMR rate is controlled by the dissociative methane adsorption over low-coordinated surface atoms [55]. A similar correlation for Ni-based catalysts has been reported before for three MgO-supported Ni catalysts with a variation of the Ni dispersion between 9% and 15% [53]. It is interesting to note that the intrinsic activity of the Rh-promoted catalysts follows the same trend as found for the non-promoted Ni catalysts. This strongly suggests that the Rh promoter is not involved in the reaction other than influencing the dispersion and reduction degree of the Ni phase.

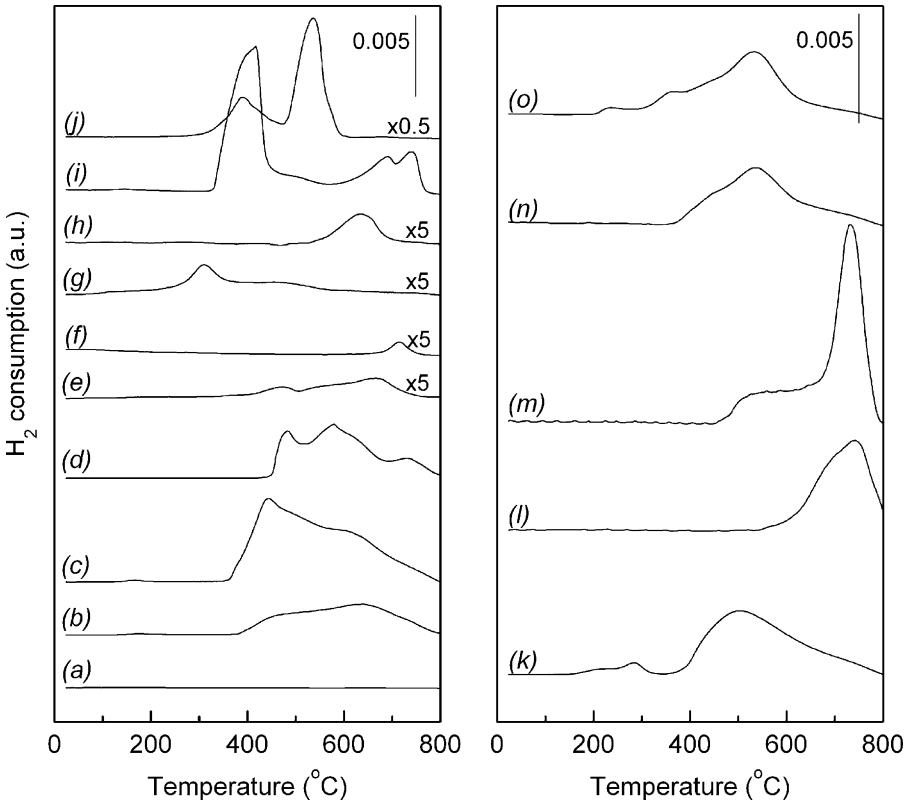

Fig. 3. TPR profiles of the (left) supports, monometallic catalysts, (right) promoted catalysts: (a) $MgAl_2O_4$, (b) Ni(20)/$MgAl_2O_4$, (c) Ni(30)/$MgAl_2O_4$, (d) Ni(20)/$MgAl_2O_4$-HDP, (e) La(10)/$MgAl_2O_4$, (f) B(2)/$MgAl_2O_4$, (g) Rh(0.5)/$MgAl_2O_4$, (h) La_2O_3, (i) Ni(20)/La_2O_3-HDP, (j) $LaNiO_3$, (k) Ni(20)La(10)/$MgAl_2O_4$, (l) Ni(20)B(1.4)/$MgAl_2O_4$, (m) Ni(30)B(2)/$MgAl_2O_4$, (n) Ni(20)Rh(0.5)/$MgAl_2O_4$, (o) Ni(20)Rh(1.6)/$MgAl_2O_4$.

A similar line of reasoning can be followed for the La-promoted catalyst, although these catalysts exhibit a slightly lower intrinsic activity. This may be due to some decoration of Ni particles by lanthana patches [16,61]. The B-promoted catalysts, on the other hand, exhibit a much higher intrinsic activity. It should be noted that the high intrinsic activity mainly derives from the correction for the low reduction degree of the catalysts. One may interpret this result in two ways. Firstly, one may argue that B promotion results in a much higher reactivity of the Ni surface atoms. Xu and Saeys [60] have argued that a surface reconstruction of the Ni terrace surface

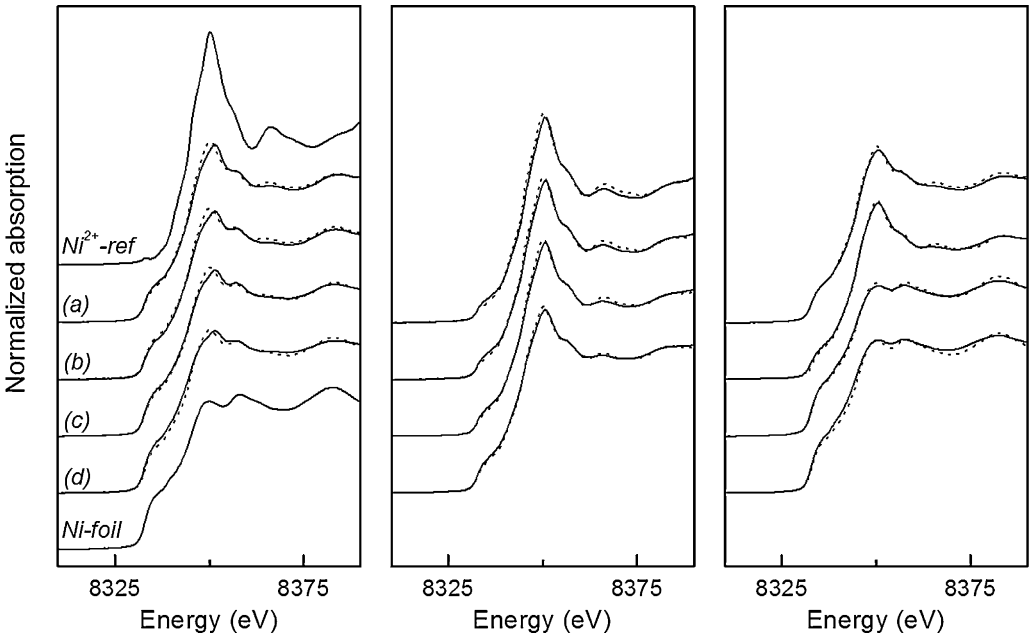

Fig. 4. Ni K-edge XANES spectra recorded of pre-reduced, passivated (left) Ni(20)/$MgAl_2O_4$-HDP, (middle) Ni(20)/$MgAl_2O_4$-DI, (right) Ni(20)La(10)/$MgAl_2O_4$. The spectra were obtained during reduction at (a) RT, (b) 200 °C, (c) 400 °C, (d) 600 °C. The fitted spectra (dotted lines) are included. The spectra of the references are those of high purity NiO and a Ni foil.

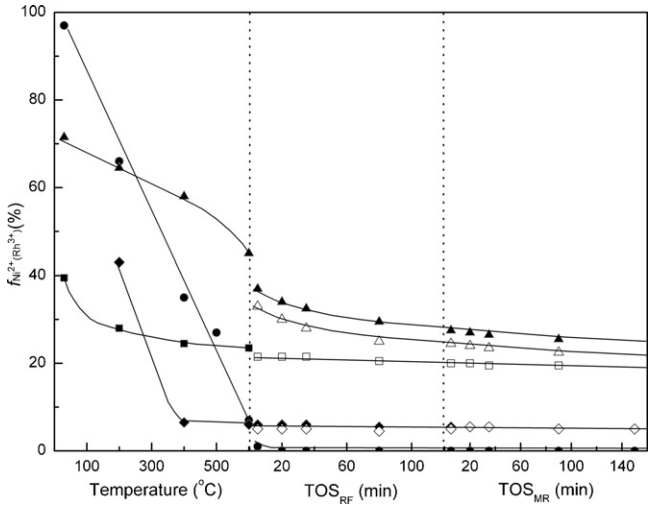

Fig. 5. Fraction of oxidic Ni (Rh) ($f_{Ni_{2+}(Rh^{3+})}$) as determined by XANES during (left) reduction, followed by (right) steam reforming at RF, MR condition at 1 bar (closed symbols), 5 bar (open symbols) of $MgAl_2O_4$-supported Ni (Rh) catalysts: Ni(20)/$MgAl_2O_4$-HDP (squares), Ni(20)/$MgAl_2O_4$ (triangles), Ni(20)La(10)/$MgAl_2O_4$ (rhombi), Rh(0.5)/$MgAl_2O_4$ (circles). Note that the Ni-based catalysts were pre-reduced, passivated, exposed to air whereas the Rh catalyst was fresh before reduction.

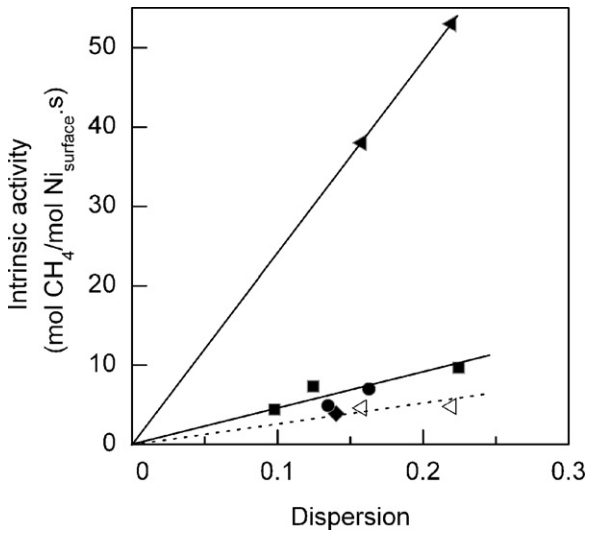

Fig. 6. Initial CH_4 steam reforming rates as function of Ni dispersion of monometallic (squares), La-promoted (rhombic), B-promoted (triangles), Rh-promoted (circles) catalysts (T = 600 °C, p = 1.2 bar, H/C = 10, O/C = 3). The initial rate is defined as the average rate between 0.5 and 2.5 h RF. The initial rate of the B-promoted catalysts under assumption of full reduction is indicated by open symbols, a dotted line.

into a more reactive steplike surface, when the octahedral sites of subsurface layers are occupied by B, leads to stronger methane adsorption and accordingly a lower barrier for methane dissociation. In this case, the linear relation between the reaction rate and the Ni dispersion of the B-promoted catalysts suggest that methane dissociation remains rate limiting. A second and alternative explanation is that an amorphous NiB_x phase is the active phase. Also in this case, the correlation between the rate and the dispersion as determined by TEM remains in place and allows to conclude that dissociative methane adsorption is rate limiting. If we assume that all Ni is involved in the SMR reaction as a nickel boride, the intrinsic rate is reasonably similar to that of the unpromoted Ni catalysts.

The effect of the promoters on the stability of a subset of the Ni catalysts during changing experimental conditions from RF and MR is illustrated in Fig. 7. These catalysts were chosen to have a nearly similar Ni dispersion and are compared to the two unpromoted Ni catalysts and Rh(0.5)/$MgAl_2O_4$. The intrinsic activity during RF is slightly higher than during MR. An explanation for this effect might be found in the much lower methane and higher carbon dioxide concentrations of MR, which results partial dry reforming. All catalysts deactivate during the SMR reaction and the non-promoted Ni catalysts seem to deactivate more than the promoted catalysts. The rate of deactivation also depends on the Ni particle size. Larger Ni particles deactivate stronger than smaller Ni particles, independent of the feed composition. This can be explained by considering coke as the main reason of deactivation. Several detailed studies have shown that large Ni particles are more prone to reaction-induced reshaping to form step-edges that act as growth sites for carbon species [17,62,63] and that they have a higher driving force for carbon diffusion due to a lower saturation concentration of carbon [64].

To compare the deactivation in a semi-quantitative manner, the slopes of the deactivation during the RF1 and MR1 condition

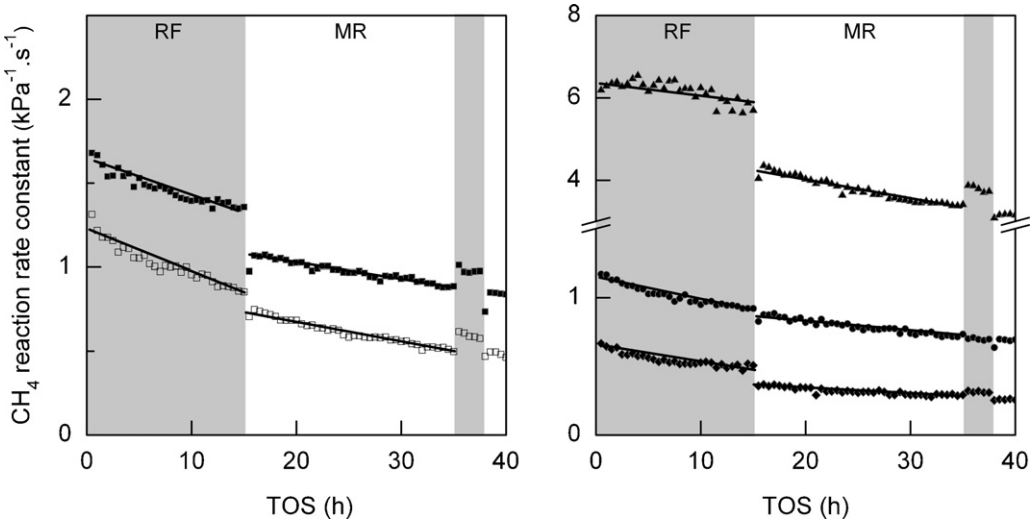

Fig. 7. CH_4 reaction rate constants as function of time on stream, during two interchanging conditions RF (T = 600 °C, p = 1.2 bar, H/C = 10, O/C = 3) and MR (T = 600 °C, p = 1.2 bar, H/C = 3, O/C = 3) of (left) monometallic (squares), (right) La-promoted (rhombi), B-promoted (triangles), Rh-promoted (circles) catalysts.

Table 4
Slopes of the deactivation (RC) during SMR under RF, MR conditions.

Catalyst	d_{av} (nm)	RC ($kPa^{-1}\ s^{-1}\ h^{-1}$)	
		RF1, 0–15 h	MR1, 15–35 h
Ni(20)La(10)/$MgAl_2O_4$	7.2	−0.016	−0.011
Ni(30)B(2)/$MgAl_2O_4$	6.4	−0.007	−0.012
Ni(20)Rh(1.6)/$MgAl_2O_4$	6.2	−0.014	−0.009
Ni(20)/$MgAl_2O_4$	8.1	−0.021	−0.018
Ni(20)/$MgAl_2O_4$-HDP	4.5	−0.012	−0.009
Rh(0.5)/$MgAl_2O_4$	1.4	−0.015	−0.017

are collected in Table 4. The deactivation during RF of the La- and Rh-promoted catalyst is nearly identical to the non-promoted Ni catalyst containing particles smaller in size. The B-promoted catalyst exhibits improved stability, whereas large Ni particles deactivate strongest. Upon exposure to MR conditions the rate of deactivation decreases, except for the B-promoted and Rh catalysts.

Recently, Sehested et al. [65–67] have discussed the contribution of sintering to deactivation of similar $MgAl_2O_4$-supported Ni catalysts at various pre-reforming conditions and formulated a model that is able to predict the sintering rate of Ni catalysts. The sintering rate is higher for the K- and S-promoted Ni catalysts only at high pressures [68]. Based on their results it is reasonable to assume that sintering is not the main cause of deactivation in the present study. This is supported by the higher rate constant of the catalysts during RF2 in comparison to the rate constant during RF1. To compare the effect of different reaction conditions for Rh(0.5)/$MgAl_2O_4$, the average particle size was determined for spent and aged Rh(0.5)/$MgAl_2O_4$, prepared by exposure to RF and 15 vol.% H_2O + 3 vol.% H_2 in He at 600 °C for 75 h, respectively. The average Rh nanoparticle size was very similar to that of the reduced catalyst, namely 1.9 ± 0.5 nm for the spent and 1.6 ± 0.4 nm for the aged catalyst. The rate of deactivation for this catalyst is comparable to that for the Ni catalysts and we may indeed conclude that sintering is not the main cause of deactivation. The B-promoted catalyst is the notable exception, which might indicate that the NiB particles have sintered and this would seem to agree with the increasing loss of activity upon comparison of the activity under RF1 and RF2 conditions (Fig. 7).

Deactivation might also be caused by oxidation of the active metallic phase during reaction as reported earlier for catalysts containing very small Rh nanoparticles [55,69]. Ni catalysts are prone to oxidation and, accordingly, H_2 is often added to the feed [70]. However, large Ni particles are more difficult to oxidize than small ones and they can also be protected for oxidation by a larger amount of carbon species. Hence, if oxidation would be the dominant reason for deactivation the small Ni particles would be expected to deactivate the fastest, which is clearly not the case (Fig. 7). For Rh-promoted catalysts it has been reported that they keep Ni in the reduced state because of the presence of a strong Ni–Rh interaction [48]. We expect that this is also the case for the La-promoted catalyst due to its similar reduction behavior. The superior stability of the B-promoted catalyst points to the absence of Ni oxidation during reaction. Therefore, further experiments were focused on the influence of the promoter on the formation of coke.

3.3. Deactivation

To investigate deactivation by coke in more detail, stimulated coking experiments were carried out. To this end, catalysts were

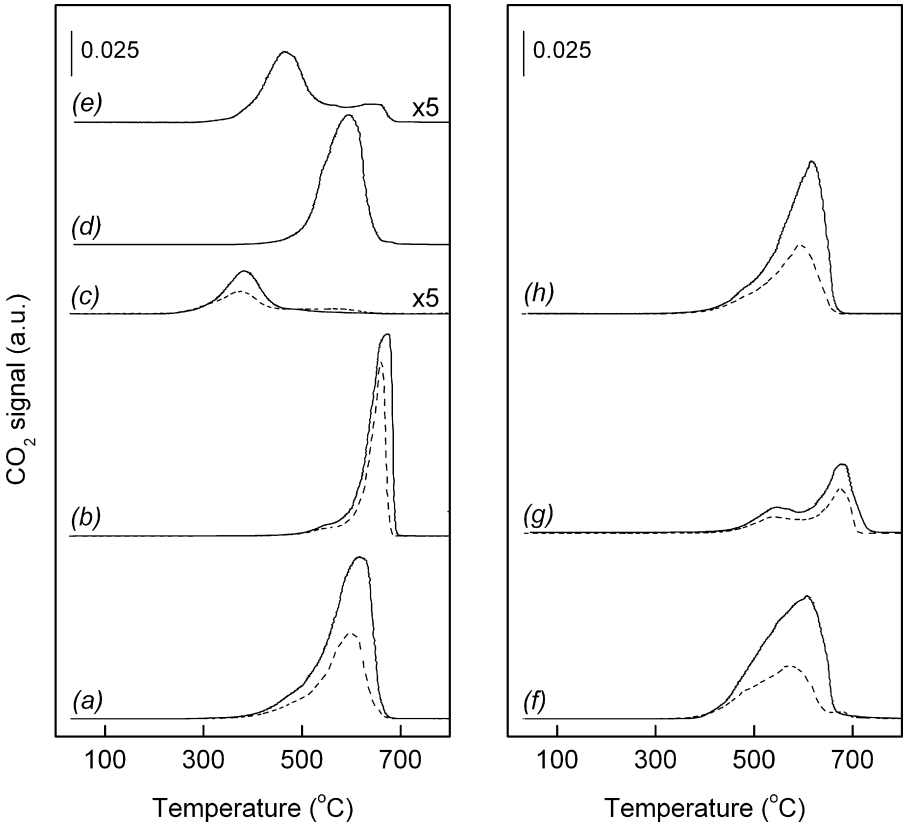

Fig. 8. TPO profiles of coked monometallic (left), promoted catalysts (right) after being exposed to 10 vol.% CH_4 in He for 5 min (dashed line), 10 min (solid line) at 600 °C. (a) Ni(20)/$MgAl_2O_4$, (b) Ni(20)/$MgAl_2O_4$-HDP, (c) Rh(0.5)/$MgAl_2O_4$, (d) Ni(20)/La_2O_3-HDP, (e) $LaNiO_3$, (f) Ni(20)La(10)/$MgAl_2O_4$, (g) Ni(30)B(2)/$MgAl_2O_4$, (h) Ni(20)Rh(1.6)/$MgAl_2O_4$.

Table 5
The amount of carbon in monometallic, promoted catalysts as determined by TPO after exposure to the indicated gas mixture (balance He) at 600 °C.

Catalyst	d_{av} (nm)	t (min)[a]	Partial pressure (bar)[b]				T_{max} (°C)	Coke (mmol/g_{cat})	Coke (mmol/mmol M_{surf})[c]
			CH_4	H_2	CO	CO_2			
Ni(20)La(10)/$MgAl_2O_4$	7.2	5	0.1	–	–	–	485, 574	9.3	23.9
		10	0.1	–	–	–	485, 611	21.3	54.6
		10	0.1	0.07	–	–	611	10.6	27.3
Ni(30)B(2)/$MgAl_2O_4$	6.4	5	0.1	–	–	–	543, 678	5.5	7.1
		10	0.1	–	–	–	547, 680	8.5	10.9
Ni(20)Rh(1.6)/$MgAl_2O_4$	6.2	5	0.1	–	–	–	485, 596	9.6	19
		10	0.1	–	–	–	485, 621	19.8	39.2
		10	0.1	0.07	–	–	625	11.1	22
Ni(20)/$MgAl_2O_4$	8.1	5	0.1	–	–	–	600	10.8	28.6
		10	0.1	–	–	–	623	21.4	56.6
		15	0.1	–	–	–	638	27.6	72.8
		10	0.1	0.03	–	–	623	15.8	41.7
		10	0.1	0.07	–	–	625	11.8	31.2
		10	0.1	0.15	–	–	631	4.2	11.1
		10	–	–	0.1	–	530	2.6	7
		10	–	–	–	0.1	242, 438	0.05	0.14
Ni(20)/$MgAl_2O_4$-HDP	4.5	5	0.1	–	–	–	663	8.7	11.9
		10	0.1	–	–	–	678	14.5	19.7
		10	0.1	0.07	–	–	669	9.5	13
		10	–	–	0.1	–	622	1.1	1.5
La(10)/$MgAl_2O_4$	–	10	0.1	–	–	–	535	0.03	–
B(2)/$MgAl_2O_4$	–	10	0.1	–	–	–	475	0.005	–
Rh(0.5)/$MgAl_2O_4$	1.4	5	0.1	–	–	–	379	0.8	17.7
		10	0.1	–	–	–	386	1.1	25.1
		10	0.1	0.07	–	–	364	0.4	10.2
		10	–	–	–	0.1	200	0.07	1.7
$MgAl_2O_4$	–	10	0.1	–	–	–	~700	0.012	–
		120	0.1	–	–	–	~500	0.005	–
Ni(20)/La_2O_3-HDP	*n.d.*	10	0.1	–	–	–	592	14.9	–
		10	0.1	0.07	–	–	577	9.3	–
$LaNiO_3$	–	10	0.1	–	–	–	468, 645	2.3	–

[a] Time of exposure.
[b] Partial pressures of gases for carbon laydown (balance He).
[c] M = Ni or Rh.

exposed to different gas mixtures at 600 °C followed by TPO to determine the amount and nature of carbonaceous deposits. Some TPO profiles of coked catalysts are displayed in Fig. 8. Coke oxidation occurs mainly between 400 and 700 °C. Carbonaceous deposits on Ni-based catalysts are typically of the type encapsulating/gum carbon, amorphous/pyrolytic carbon (thin CH_x films or a few layers of Ni covering graphite) and carbon whisker (filaments) [17]. The oxidation of amorphous carbonaceous deposits occurs at relatively low temperature, whilst graphitic carbon is oxidized at high temperature [21].

Table 5 collects the amount of carbon deposited during exposure to different gas mixtures at 600 °C followed by TPO. The total amount of carbon as well as the ratio of carbon per surface atom evidences that the dominant source of coke is CH_4, because the coke deposits formed by dissociative adsorption of CH_4 are about one order of magnitude greater in amount than those generated by CO. The amount of coke formed by decomposition of CO_2 is even lower. Ni(20)/$MgAl_2O_4$ is more susceptible to form coke than its counterpart prepared by HDP. With increased time of exposure to methane the reactivity of the carbonaceous deposits towards oxidation is greatly reduced. The decomposition of methane with hydrogen reduces the amount of carbon deposits formed and can therefore partially prevent encapsulation and thus deactivation of the catalyst.

The coking propensity of Ni-free promoter-containing supports is negligible and similar to that of the bare support, expect for Rh(0.5)/$MgAl_2O_4$. This catalyst has about three times more carbon per surface Rh atom at 600 °C than formed at 500 °C. The temperature of coke oxidation on Ni is more than 200 °C higher than on Rh, showing the better resistance against coking of the more noble metal.

The amounts of coke on Ni(20)/$MgAl_2O_4$-HDP and Ni(20)/La_2O_3-HDP are quite similar. The coke on Ni(20)/La_2O_3-HDP is easier to oxidize. It points to the interaction of Ni with La on the support. The amount of coke formed and its reactivity towards oxidation of Ni(20)La(10)/$MgAl_2O_4$ does not significantly differ from the unpromoted catalyst. These results are expected because the formation of coke on La-containing catalysts is supposed to be suppressed by a higher gasification rate of carbon with adsorbed CO_2 present in the form of $La_2O_2CO_3$-type species [38,71]. High amounts of strongly binding carbonates may hinder the SMR reaction by slowing regeneration of these active sites. Indeed, a more intense and significantly broader peak is found in the CO_2-TPD profile of Ni(20)La(10)/$MgAl_2O_4$ in comparison to Ni(20)/$MgAl_2O_4$ (not shown), which demonstrates that the basicity is increased. XRD (not shown) of carbonated La_2O_3 revealed the transformation of La_2O_3 into $La_2O_2CO_3$-type species. From these results we can reason that a change in the concentration of oxycarbonate species by the higher CO_2 partial pressure in MR led to a decrease of deactivation.

The amount of carbonaceous deposits formed on the B-promoted catalyst is low taken into account its activity. Two peaks

are visible in the TPO profile centered around 545 and 680 °C. By comparison to the profiles of non-promoted catalysts, the use of B greatly reduces the formation of more difficult to oxidize carbon deposits. This is in line with its higher stability during SMR and it could reflect a selective blockage of subsurface and step sites for the initiation of carbon formation by B [41]. The amount of coke formed on the Rh-promoted catalyst is slightly lower than of Ni(20)/$MgAl_2O_4$, which could be the result of the higher hydrogenation activity of Rh, in addition to alloy species [72]. Overall, the amount of carbonaceous deposits increases in the order B < no promoter-HDP < Rh < La ∼ no promoter.

4. Conclusions

The reaction rate of Ni-based reforming catalysts increases linearly with the Ni dispersion. Accordingly, it is important to employ highly dispersed Ni to obtain sufficiently active Ni-based catalysts for energy-efficient membrane reforming of methane. Such small Ni particles may be obtained by standard deposition-precipitation techniques or the use of B as a promoter. In comparison, La and Rh as promoters have a smaller effect on the Ni particle size. The degree of Ni reduction depends on the particle size and the additive. Small Ni particles cannot be fully reduced, especially in the presence of B. The degree of reduction strongly increases if Ni is in contact with La or Rh. The initial intrinsic rate per surface metal atom increases linearly with the Ni metal dispersion for Ni, NiLa and NiRh catalysts. This implies that the La and Rh promoters do not participate in the reaction and only modify the Ni particle size. The catalysts modified by B show a much higher surface atom based activity if it is assumed that only reduced Ni sites participate in the reaction. If a NiB_x phase is assumed to be active, the intrinsic activity of NiB catalysts is similar to that of the other catalysts. Catalyst stability increases in the order La < Rh < B. Deactivation of the catalysts is caused by insufficient removal of carbon species from the surface of Ni particles and the formation of stable, graphitic carbon deposits, most likely covering the surface of metal. This effect is suppressed for smaller Ni particles. Consequently, the effect of the additives can be explained by the way they affect the generation or removal of deactivating carbon species. B is an excellent structural promoter to obtain small Ni particles, Rh stabilizes metallic Ni and La can remove some of the carbon deposits more effectively by gasification. Only the B promoter has a very favorable influence on the Ni dispersion and its stability to steam methane reforming at a moderate operation temperature. Despite the inhibition of Ni reduction by B, B-promoted Ni catalysts show similar weight-based reaction rates as a standard Ni catalyst of similar dispersion but with improved stability.

Acknowledgements

This research was performed within the framework of the EOS-LT program. The authors gratefully acknowledge Agentschap NL of the Netherlands Ministry of Economic Affairs for financial support, NWO-Dubble for access to X-ray absorption spectroscopy facilities at ESRF, ESRF staff for their support and the Soft Matter Cryo-TEM Research Unit for access to the TEM facility. We thank Mrs. Adelheid Elemans for the elemental analysis and Mr. Xian-Yang Quek for the TEM measurements.

References

[1] J.R. Rostrup-Nielsen, T. Rostrup-Nielsen, Cattech 6 (2002) 150.
[2] R. Schlögl, Angew. Chem. Int. Ed. 42 (2003) 42–43.
[3] H. Li, J.W. Dijkstra, J.A.Z. Pieterse, J. Boon, R.W. van den Brink, D. Jansen, J. Membr. Sci. 363 (2010) 204–205.
[4] J.A.Z. Pieterse, J. Boon, Y.C. van Delft, J.W. Dijkstra, R.W. van den Brink, Catal. Today 156 (2010) 153–164.
[5] J. Sehested, Catal. Today 111 (2006) 103–110.
[6] J.G. Jakobsen, T.L. Jørgensen, I. Chorkendorff, J. Sehested, Appl. Catal. A 377 (2010) 158–166.
[7] M.C.J. Bradford, M.A. Vannice, J. Catal. 183 (1999) 69–75.
[8] A. Erdöhelyi, J. Cserényi, F. Solymosi, J. Catal. 141 (1993) 287–299.
[9] M.F. Mark, W.F. Maier, J. Catal. 164 (1996) 122–130.
[10] W. Cai, F. Wang, E. Zhan, A.C. van Veen, C. Mirodatos, W. Shen, J. Catal. 257 (2008) 96–107.
[11] J.H. Bitter, K. Seshan, J.A. Lercher, J. Catal. 171 (1997) 279–286.
[12] S.M. Stagg-Williams, F.B. Noronha, G. Fendley, D.E. Resasco, J. Catal. 194 (2000) 240–249.
[13] A. Yamaguchi, E. Iglesia, J. Catal. 274 (2010) 52–63.
[14] J.R. Rostrup-Nielsen, Steam Reforming Catalysts, Danish Technical Press, Copenhagen, 1975.
[15] J.K. Nørskov, S. Holloway, N.D. Lang, Surf. Sci. 137 (1984) 65–78.
[16] J.R. Rostrup-Nielsen, J. Sehested, J.K. Nørskov, Adv. Catal. 47 (2002) 85–133.
[17] H.S. Bengaard, J.K. Norskov, J. Sehested, B.S. Clausen, L.P. Nielsen, A.M. Molenbroek, J.R. Rostrup-Nielsen, J. Catal. 209 (2002) 365–384.
[18] H.S. Bengaard, I. Alstrup, I. Chorkendorff, S. Ullmann, J.R. Rostup-Nielsen, J.K. Nørskov, J. Catal. 187 (1999) 238–244.
[19] J.R. Rostup-Nielsen, J. Catal. 85 (1984) 31–43.
[20] F. Besenbacher, I. Chorkendorff, B.S. Clausen, B. Hammer, A.M. Molenbroek, J.K. Nørskov, I. Stensgaard, Science 279 (1998) 1913–1915.
[21] D.L. Trimm, Catal. Today 49 (1999) 3–10.
[22] E. Nikolla, J. Schwank, S. Linic, J. Catal. 250 (2007) 85–93.
[23] J. Xu, L. Chen, K.F. Tan, A. Borgna, M. Saeys, J. Catal. 261 (2009) 158–165.
[24] M. Nowosielska, W.K. Jóźwiak, J. Rynkowski, Catal. Lett. 128 (2009) 83–93.
[25] J.C.S. Wu, H.-C. Chou, Chem. Eng. J. 148 (2009) 541–544.
[26] M. Nurunnabi, Y. Mukainakano, S. Kado, B. Li, K. Kunimori, K. Suzuki, K. Fujimoto, K. Tomishige, Appl. Catal. A 299 (2006) 152.
[27] B. Li, S. Kado, Y. Mukainakano, T. Miyazawa, T. Miyao, S. Naito, K. Okumura, K. Kunimori, K. Tomishige, J. Catal. 245 (2007) 144–155.
[28] M. García-Diéguez, E. Finocchio, M.Á. Larrubia, L.J. Alemany, G. Busca, J. Catal. 274 (2010) 13.
[29] M. Nurunnabi, Y. Mukainakano, S. Kado, T. Miyazawa, K. Okumura, T. Miyao, S. Naito, K. Suzuki, K. Fujimoto, K. Kunimori, K. Tomishige, Appl. Catal. A 308 (2006) 1.
[30] M. García-Diéguez, M.C. Herrera, I.S. Pieta, M.Á. Larrubia, L.J. Alemany, Catal. Commun. 11 (2010) 1133–1136.
[31] R. Martínez, E. Romero, C. Guimon, R. Bilbao, Appl. Catal. A 274 (2004) 139–149.
[32] Y. Cui, H. Zhang, H. Xu, W. Li, Appl. Catal. A 331 (2007) 60–69.
[33] R. Yang, C. Xing, C. Lv, L. Shi, N. Tsubaki, Appl. Catal. A 385 (2010) 92–100.
[34] J.R. Rostrup-Nielsen, J.H. Bak Hansen, J. Catal. 144 (1993) 43–45.
[35] T. Horiuchi, K. Sakuma, T. Fukui, Y. Kubo, T. Osaki, T. Mori, Appl. Catal. A 144 (1996) 111–120.
[36] J.R. Rostrup-Nielsen, J. Catal. 33 (1974) 184.
[37] J. Guo, H. Lou, H. Zhao, D. Chai, X. Zheng, Appl. Catal. A 273 (2004) 75.
[38] Z. Zhang, X.E. Verykios, Appl. Catal. A 138 (1996) 109–133.
[39] S. Kurungot, T. Yamaguchi, Catal. Lett. 92 (2004) 181–187.
[40] M.C. Sánchez-Sánchez, R.M. Navarro, J.L.G. Fierro, Catal. Today 129 (2007) 336–345.
[41] J. Xu, M. Saeys, J. Catal. 242 (2006) 217–226.
[42] L. Chen, Y. Lu, Q. Hong, J. Lin, F.M. Dautzenberg, Appl. Catal. A 292 (2005) 296–299.
[43] M. Ferrandon, A.J. Kropf, T. Krause, Appl. Catal. A 379 (2010) 121–128.
[44] F. Basile, G. Fornasari, F. Trifirò, Catal. Today 77 (2002) 215–223.
[45] Z. Hou, T. Yashima, Catal. Lett. 89 (2003) 193–197.
[46] C.H. Bartholomew, A.H. Uken, Appl. Catal. 4 (1982) 19–29.
[47] Y. Chen, C. Xie, Y. Li, C. Song, T.B. Bolin, Phys. Chem. Chem. Phys. 12 (2010) 5709.
[48] J.J. Strohm, J. Zheng, C. Song, J. Catal. 238 (2006) 314–317.
[49] J.A.Z. Pieterse, Personal communication.
[50] M.E. Rivas, J.L.G. Fierro, M.R. Goldwasser, E. Pietri, M.J. Pérez-Zurita, A. Griboval-Constant, G. Leclercq, Appl. Catal. A 344 (2008) 11–14.
[51] T. Le Van, M. Che, J.M. Tatibouët, M. Kermarec, J. Catal. 142 (1993) 18.
[52] S. Bernal, G.A. Martin, P. Moral, V. Perrichon, Catal. Lett. 6 (1990) 232.
[53] J. Wei, E. Iglesia, J. Catal. 224 (2004) 370–383.
[54] J. Zhang, H. Xu, X. Jin, Q. Ge, W. Li, Appl. Catal. A 290 (2005) 89–91.
[55] D.A.J.M. Ligthart, R.A. van Santen, E.J.M. Hensen, J. Catal. 280 (2011) 206–220.
[56] R. Burch, P.K. Loader, N.A. Cruise, Appl. Catal. A 147 (1996) 378–380.
[57] J. Requies, M.A. Cabrero, V.L. Barrio, M.B. Güemez, J.F. Cambra, P.L. Arias, F.J. Pérez-Alonso, M. Ojeda, M.A. Peña, J.L.G. Fierro, Appl. Catal. A 289 (2005) 217.
[58] H. Li, H. Li, J.F. Deng, Catal. Today 74 (2002) 57–60.
[59] J. Legrand, A. Taleb, S. Gota, M.-J. Guittet, C. Petit, Langmuir 18 (2002) 4131–4137.
[60] J. Xu, M. Saeys, J. Phys. Chem. C 113 (2009) 4099–4106.
[61] S. Bernal, J.J. Calvino, C. López-Cartes, J.M. Pintado, J.A. Pérez-Omil, J.M. Rodríguez-Izquierdo, K. Hayek, G. Rupprechter, Catal. Today 52 (1999) 40–41.
[62] S. Helveg, C. López-Cartes, J. Sehested, P.L. Hansen, B.S. Clausen, J.R. Rostrup-Nielsen, F. Abild-Pedersen, J.K. Nørskov, Nature 427 (2004) 426–430.
[63] A.M. Molenbroek, S. Helveg, H. Topsøe, B.S. Clausen, Top. Catal. 52 (2009) 1306–1308 (references therein).
[64] K.O. Christensen, D. Chen, R. Lødeng, A. Holmen, Appl. Catal. A 314 (2006) 13–15.
[65] J. Sehested, J.A.P. Gelten, I.N. Remediakis, H. Bengaard, J.K. Norskov, J. Catal. 223 (2004) 432–443.
[66] J. Sehested, J. Catal. 217 (2003) 417–426.
[67] J. Sehested, A. Carlsson, T.V.W. Janssens, P.L. Hansen, A.K. Datye, J. Catal. 197 (2001) 200–209.

[68] J. Sehested, J.A.P. Gelten, S. Helveg, Appl. Catal. A 309 (2006) 237–246.
[69] D.A.J.M. Ligthart, R.A. van Santen, E.J.M. Hensen, Angew. Chem. Int. Ed. 50 (2011) 5306–5310.
[70] Y.-H. Chin, D.L. King, H.-S. Roh, Y. Wang, S.M. Heald, J. Catal. 244 (2006) 160.
[71] M. Benito, S. García, P. Ferreira-Aparicio, L. García Serrano, L. Daza, J. Power Sources 169 (2007) 181–182.
[72] M. Nurunnabi, Y. Mukainakano, S. Kado, T. Miyao, S. Naito, K. Okumura, K. Kunimori, K. Tomishige, Appl. Catal. A 325 (2007) 154.